Intrinsic thermal conductivities and size effect of alloys of wurtzite AlN, GaN, and InN from first-principles

Jinlong Ma,[1] Wu Li,[2,a)] and Xiaobing Luo[1,b)]
[1]*State Key Laboratory of Coal Combustion, School of Energy and Power Engineering, Huazhong University of Science and Technology, Wuhan 430074, China*
[2]*Institute for Advanced Study, Shenzhen University, Shenzhen 518060, China*

(Received 5 January 2016; accepted 14 March 2016; published online 23 March 2016)

Despite the fact the alloys of wurtzite AlN, GaN, and InN are widely used in electronics, the studies on their thermal conductivities (κ) are inadequate, and the intrinsic limits are still unknown. In this work, the intrinsic κ of alloys and their films are calculated from first-principles within the virtual crystal treatment. The κ of alloys are strongly suppressed even by a small amount of alloying. For instance, with only 1% alloying of Al or In, κ of GaN decreases about 60%. At relatively high alloying, with concentration between 0.2 and 0.8, the κ of alloys are not significantly changed. At room temperature, the minimal *a*-axis κ are about 18, 22, and 8 $\mathrm{W\,m^{-1}\,K^{-1}}$, while the minimal *c*-axis κ are about 22, 27, and 10 $\mathrm{W\,m^{-1}\,K^{-1}}$ for $Al_xGa_{1-x}N$, $In_xGa_{1-x}N$, and $In_xAl_{1-x}N$, respectively. The size effect in films can persist up to a few tens of micrometers, and κ can be reduced by half in about 100 nm thick films. © *2016 AIP Publishing LLC*.
[http://dx.doi.org/10.1063/1.4944809]

I. INTRODUCTION

The alloys of wurtzite AlN, GaN, and InN have been widely used in electronic and optoelectronic devices, such as transistors,[1–3] light emitting diodes,[4–6] laser diodes,[7–9] and solar cells.[10–12] In these applications, the thermal conductivities (κ) of these alloys play an important role in the efficiency of heat dissipation, which is crucial for the device performance and reliability. The κ of $Al_xGa_{1-x}N$ films,[13–15] $In_xGa_{1-x}N$ films,[16–18] and $In_xAl_{1-x}N$ films[19,20] have been experimentally measured, showing strong dependence of κ on the sample qualities. Therefore, the intrinsic limits of κ in clean and bulk alloys are still unknown. *Ab initio* calculations have demonstrated high accuracy in predicting κ for clean systems.[21–24] For instance, we found that κ of bulk InN can reach as high as 130–150 $\mathrm{W\,m^{-1}\,K^{-1}}$, in line with the latest measured value of 120 $\mathrm{W\,m^{-1}\,K^{-1}}$ on high-quality InN films,[25] which is almost three times larger than the first reported value[26] of 45 $\mathrm{W\,m^{-1}\,K^{-1}}$.

In this work, the intrinsic κ of bulk $Al_xGa_{1-x}N$, $In_xGa_{1-x}N$, and $In_xAl_{1-x}N$ and their films are studied with the first-principles calculation combined with the virtual crystal method.[27–29] The alloying and size effect on thermal transport are investigated. Because of the large atomic mass difference between cations, κ of these alloys are greatly decreased due to the strong mass disorder. The size effect is stronger for the alloys than for pure compounds in thick samples; however, it is weaker in alloys than in pure compounds in thin samples. The size effect in films can persist up to a few tens of micrometers, and κ can be reduced by half in about 100 nm thick films.

II. METHODOLOGY

The thermal conductivity can be obtained by solving the phonon Boltzmann transport equation (BTE). At temperature T, it can be written as[30]

$$\kappa^{\alpha\beta} = \frac{1}{k_B T^2 NV} \sum_{\lambda} (\hbar\omega_\lambda)^2 f_\lambda^0 \left(1 + f_\lambda^0\right) v_\lambda^\alpha F_\lambda^\beta, \tag{1}$$

where k_B is the Boltzmann constant and $\hbar$ is the reduced Planck constant. λ denotes a phonon mode specified by wave vector $\mathbf{q}$ and branch index p. N is the number of $\mathbf{q}$ meshes of the Brillouin zone, and V is the volume of the unit cell. α and β are the Cartesian directions. ω_λ is the angular frequency, v_λ is the group velocity, and f_λ^0 is the Bose-Einstein distribution function. F_λ^β is the β component of the mean free displacement $\mathbf{F}_\lambda$, which can be obtained from the phonon BTE.[30]

To calculate the intrinsic κ of alloys, the alloy scattering is required in addition to the three-phonon scattering and natural isotope scattering.[30] Here, the frequently used virtual crystal model is adopted to calculate the alloy scattering.[27–29] In the virtual crystal assumption, the alloy is assumed to have a similar crystal structure of its constituent compounds, with averaged lattice parameters, atomic masses, and interatomic force constants (IFCs) based on the constituent concentration. Moreover, the alloy scattering probability is assumed to dominantly result from the mass disorder and is then calculated in the same way as isotope scattering[27–29]

$$\Gamma_{\lambda\lambda'} = \frac{\pi\omega^2}{2} \sum_{i \in u.c.} g(i) |\mathbf{e}_\lambda^*(i) \cdot \mathbf{e}_{\lambda'}(i)|^2 \delta(\omega_\lambda - \omega_{\lambda'}), \tag{2}$$

where $g(i) = \sum_s f_s(i)[1 - M_s(i)/\bar{M}(i)]^2$ is the mass variance with $f_s(i)$ and $M_s(i)$ being the concentration and mass of the

a)Electronic mail: wu.li.phys2011@gmail.com
b)Electronic mail: luoxb@hust.edu.cn

sth constituent atom, and $\bar{M}(i)$ being the average mass of the ith atom in the unit cell. $\mathbf{e}_\lambda(i)$ is the eigenvector of the mode λ at the ith atom, while the asterisk denotes the complex conjugate. The δ function ensures the energy conservation.[30]

In the case of thin film, the phonon BTE becomes space dependent[31] and needs to be solved under specific boundary condition, which usually refers to diffusive boundary condition. Conventionally, Matthiessen's rule is used to combine boundary scattering and other scatterings in a simple way,[32] which has been proven inaccurate in two-dimension ribbons.[33] Under relaxation time approximation (RTA),[31,32] namely, $\mathbf{F}_\lambda^{\mathrm{RTA}} = \mathbf{v}_\lambda \tau_\lambda$ with τ_λ being the relaxation time for bulk, analytical solution of the space-dependent BTE exists under diffusive boundary condition. For in-plane transport in films, the averaged space-dependent relaxation time can be analytically obtained as[30–32]

$$\begin{aligned}\bar{\tau}_\lambda &= \frac{\tau_\lambda}{L}\int_0^L \left\{1 - e^{-|(L-l)/\tau_\lambda v_\lambda^z|}\right\} dl, \\ &= \tau_\lambda \left[1 - \frac{|\tau_\lambda v_\lambda^z|}{L}\left(1 - e^{-L/|\tau_\lambda v_\lambda^z|}\right)\right], \end{aligned} \tag{3}$$

where z denotes the transport direction, and L is the film thickness. The thickness direction is taken as c-axis of the wurtzite structure in the calculations performed in this work. κ of thin film can be then obtained with $\mathbf{F}_\lambda = \mathbf{v}_\lambda \bar{\tau}_\lambda$ in Eq. (1).

We use the same IFCs for AlN and InN as in our previous works,[23,25] and the IFCs calculations for GaN follow the same methodology. The calculations of the IFCs are performed using VASP[34] with local density approximation (LDA)[35] and projector augmented wave (PAW) pseudopotentials.[36] The Phonopy package[37] is used to extract the harmonic IFCs, and the ShengBTE package[30] is used to obtain the third-order anharmonic IFCs and solve the BTE.

III. RESULTS AND DISCUSSION

Wurtzite AlN and InN have already been studied with the same IFCs in the previous works.[23,25] However, the phonon dispersion of wurtzite AlN was not shown in Ref. 23. For completeness, it is given in Fig. 1(a), where excellent agreement with the experiment[38] can be seen.

The relaxed lattice constants of wurtzite GaN are $a = 3.158$ Å and $c = 5.148$ Å, slightly smaller than the experimental values,[39] $a_{exp} = 3.190$ Å and $c_{exp} = 5.189$ Å. The calculated phonon dispersion, as plotted in Fig. 1(b), agrees well with the measurements.[40,41] Figure 2(a) shows the a-axis and c-axis κ of naturally occurring wurtzite GaN, with isotope concentration as 60.1% ^{69}Ga and 39.9% ^{71}Ga for gallium and 99.6% ^{14}N and 0.4% ^{15}N for nitrogen, where the calculated a-axis κ are in good agreement with the measured values along a-axis.[42] At room temperature, the calculated a-axis and c-axis κ are 244 $\mathrm{W\,m^{-1}\,K^{-1}}$ and 279 $\mathrm{W\,m^{-1}\,K^{-1}}$, respectively, giving an anisotropy of about 14%. As temperature increases from 150 K to 500 K, the anisotropy reduces monotonically from 23% to 13%, revealing that the anisotropy of wurtzite GaN cannot be neglected, especially at low temperatures. This is in contrast to the work by Lindsay *et al.*, which shows almost isotropic thermal conductivities.[43]

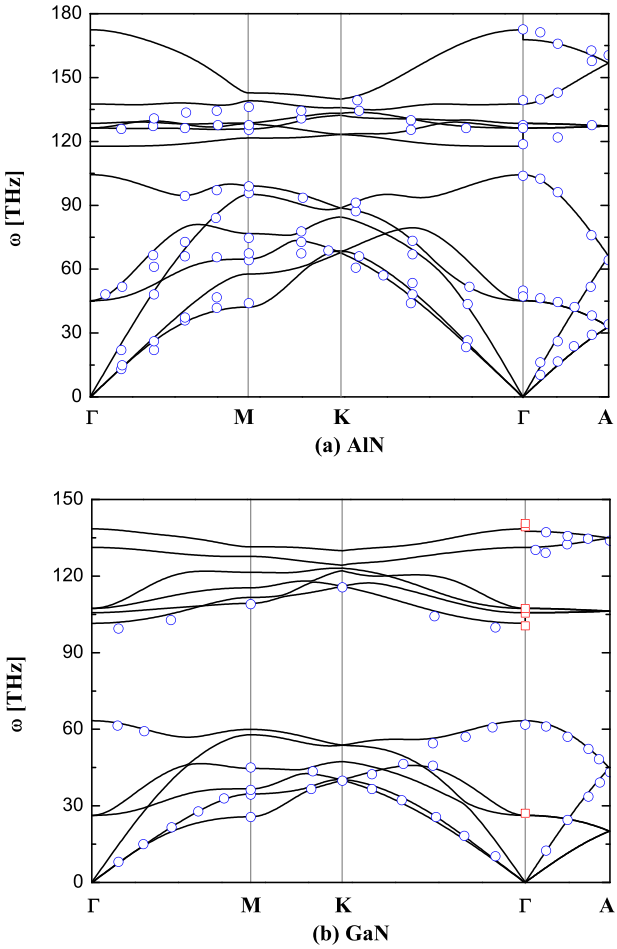

FIG. 1. Calculated phonon dispersions along several high-symmetry directions for (a) AlN and (b) GaN. The circles in (a) correspond to X-ray scattering measurements.[38] The circles and squares in (b) correspond to X-ray scatting[40] and Raman measurements,[41] respectively.

As we revealed in Ref. 25, the anisotropy of κ derives from the anisotropy of the mode-averaged group velocity squared, though the group velocities along a-axis and c-axes are almost the same. The averaged square of velocity can be calculated with $v^2_{\omega,\alpha} = \sum_\lambda v^2_{\lambda,\alpha}\delta(\omega - \omega_\lambda)/\sum_\lambda \delta(\omega - \omega_\lambda)$. Figure 2(b) shows the v^2_ω along the a-axis and c-axis directions of GaN. At low-frequency limit, the constant v^2_ω are about 7.30 and 9.17 $(\times 10^3\,\mathrm{m/s})^2$ for a-axis and c-axis directions, respectively, showing an anisotropy of about 26%. Even at 500 K, more than 95% of κ are contributed from phonons below 50 THz, as revealed from Fig. 2(c), which then dominate the anisotropy of κ. As shown in Fig. 2(b), the anisotropy at intermediate frequencies is smaller than that at low frequencies. As a consequence, the anisotropy of κ increases with decreasing temperature, due to increased contribution from low-frequency phonons. The large anisotropy at low frequencies mainly comes from the high-transverse acoustic (TA2) phonons rather than the low-transverse acoustic (TA1) and longitudinal acoustic (LA) modes, as revealed in the inset of Fig. 2(b). The low-frequency limits of a-axis and c-axis v^2_ω are about 5.41 vs 5.32 $(\times 10^3\,\mathrm{m/s})^2$ for TA1, 7.53 vs 12.65 $(\times 10^3\,\mathrm{m/s})^2$ for TA2, and 18.39 vs 19.00 $(\times 10^3\,\mathrm{m/s})^2$ for LA, with an anisotropy of about 2%, 68%, and 3%, respectively.

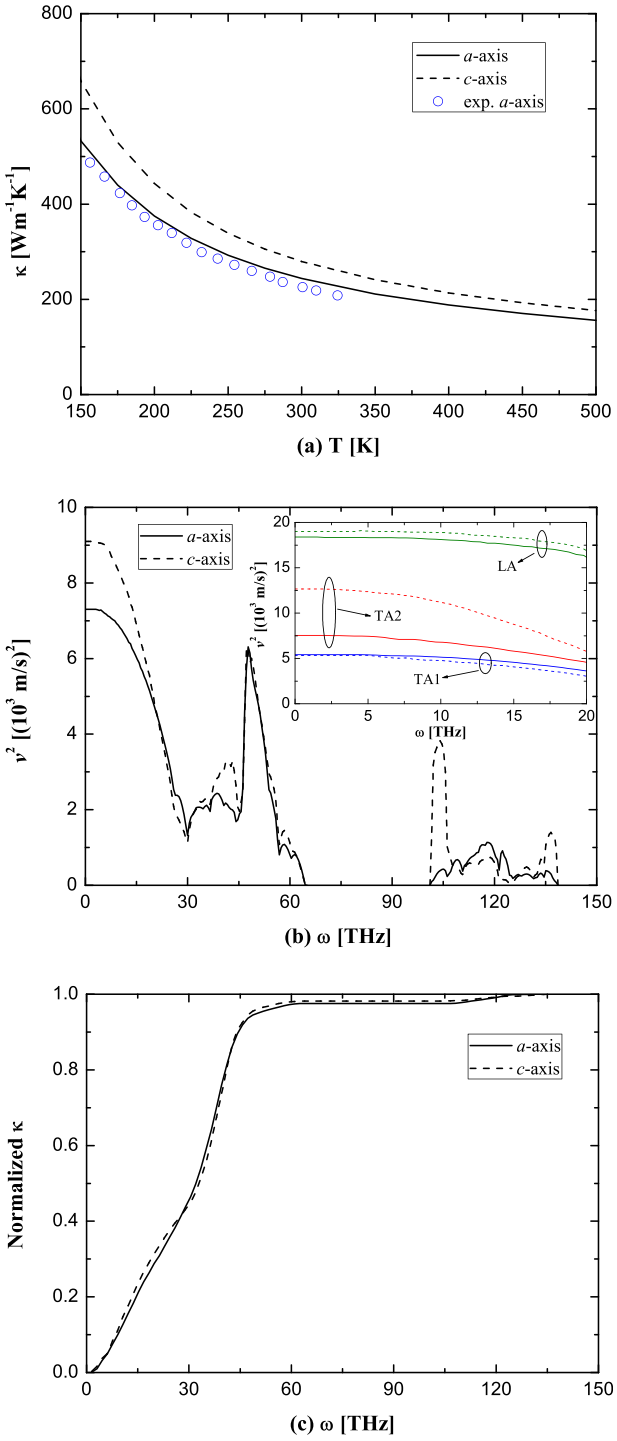

FIG. 2. (a) Calculated a-axis and c-axis thermal conductivities of GaN, in comparison with a-axis experimental data measured for a sample with a thickness of 200 μm.[42] (b) The averaged square of phonon velocities in GaN along a-axis and c-axis directions. The inset shows the a-axis (solid line) and c-axis (dashed line) values of low-frequency TA1, TA2, and LA phonons, respectively. (c) Normalized cumulative thermal conductivities of GaN vs angular frequency at 500 K.

For alloys, the dependence of intrinsic κ on alloying concentration is investigated, as shown in Fig. 3. It is found that κ of alloys decrease significantly even with a small amount of alloying. For instance, the a-axis and c-axis κ of $Al_{0.01}Ga_{0.99}N$ are 99 and 118 W m^{-1} K^{-1}, respectively, about 60% and 58% decrease compared with GaN. While for

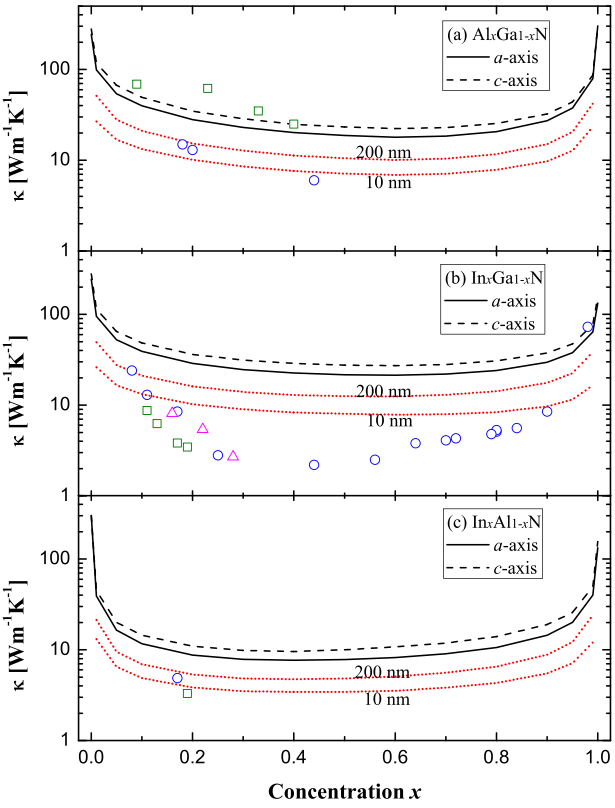

FIG. 3. The calculated a-axis and c-axis thermal conductivities at room temperature vs alloy concentration for (a) $Al_xGa_{1-x}N$, (b) $In_xGa_{1-x}N$, and (c) $In_xAl_{1-x}N$. The dotted lines are calculated a-axis thermal conductivities for 10 nm-thick and 200 nm-thick films, respectively. In (a), the circles are measurements of thin films[13] and the squares are experimental data for thick films with thickness of 0.3–0.7 μm.[15] In (b), the circles, squares, and triangles are experimental measurements of films with thickness of 147–4600 nm,[18] 81–190 nm,[17] and ~110 nm,[16] respectively. In (c), the circle is measured data for ~200 nm-thick film[19] and the square is measured data also for ~200 nm-thick film.[20]

$In_{0.01}Ga_{0.99}N$, the a-axis and c-axis κ are 95 and 115 W m^{-1} K^{-1}, respectively, about 61% and 59% lower than those of GaN. Actually at such slight alloying, the phonon frequency, group velocity, and anharmonic scattering are almost not affected. The reduction of κ mainly comes from the alloy scattering due to large mass disorder between the cations. When the alloying concentration varies between 0.2 and 0.8, the reduction of κ does not change significantly, being consistent with Si_xGe_{1-x} alloy,[27,44,45] $PbSe_xTe_{1-x}$ alloy,[28] and $Mg_2Si_xSn_{1-x}$ alloy.[29] The minimal a-axis κ and c-axis κ are about 18 and 22 W m^{-1} K^{-1} for $Al_xGa_{1-x}N$, 22 and 27 W m^{-1} K^{-1} for $In_xGa_{1-x}N$, and 8 and 10 W m^{-1} K^{-1} for $In_xAl_{1-x}N$, respectively. The anisotropy of alloys then exceeds 20%, larger than that of pure compounds. This stems from the weaker suppression due to alloy effect on low-frequency phonons, which have larger anisotropy than high-frequency phonons. In Fig. 3, the experimental values are also plotted for comparison. It can be seen that the calculated intrinsic κ are generally larger than the experiments. This is reasonable as the experimental values are often obtained from thin films with a thickness less than 1 μm.[14,16,18–20] Therefore, the boundary scattering also plays a role in these samples. We also calculate κ of films with a thickness of 200 nm and 10 nm. The calculated κ of films can only

coincide with some of the experiments but have apparent difference with the others. The discrepancy can be expected due to the unconsidered sample-dependent scatterings, such as impurities[17] or dislocations,[13] and the compositional inhomogeneities effect especially at heavy alloying.[18] The calculated results represent the upper limits of thermal conductivities in clean samples.

In order to have a quantitative understanding of the size effect, the normalized a-axis κ of GaN and $In_{0.5}Ga_{0.5}N$ as a function of the film thickness are plotted in Fig. 4 for room temperature. The calculation reveals that the size effect can persist up to a few tens of micrometers. The size effect is related to the mean free paths (MFPs) distribution, which can be reflected in the normalized cumulative κ vs MFPs[22,29,30] (also plotted in Fig. 4). It can be seen that the MFPs of heat-conductive phonons in GaN mainly range between 10 nm and 10 μm, which accounts for about 95% thermal conductivity. As the alloy effect has stronger influence on high-frequency phonons with small MFPs than low-frequency phonons with large MFPs, the relative contribution from large MFPs in alloys is increased as compared with its constituent compounds. Since boundary suppresses the contribution of phonons with MFPs larger than or similar to boundary size, the size effect is stronger in alloys than in pure compounds in thick samples. On the other hand, there are more phonon modes with MFPs smaller than a given short MFP in alloys, resulting in a larger fraction of heat conducted by modes with short MFPs.[29] As a consequence, the normalized cumulative κ curve of $In_{0.5}Ga_{0.5}N$ crosses with that of GaN at intermediate MFPs. Correspondingly, their normalized κ vs thickness curves also cross. Unlike in Si,[22] Mg_2Si, and Mg_2Sn nanowires,[29] κ of films agree with the cumulative κ with respect to MFPs only qualitatively but not quantitatively. The boundary scattering in films is weaker than that in nanowires with a diameter equal to the film thickness. The cumulative κ vs MFPs function overestimates the size effect in films. Further calculations show that both the normalized κ vs thickness and the normalized cumulative κ vs MFPs for AlN, InN, and other alloys are quite similar to those for GaN and $In_{0.5}Ga_{0.5}N$.

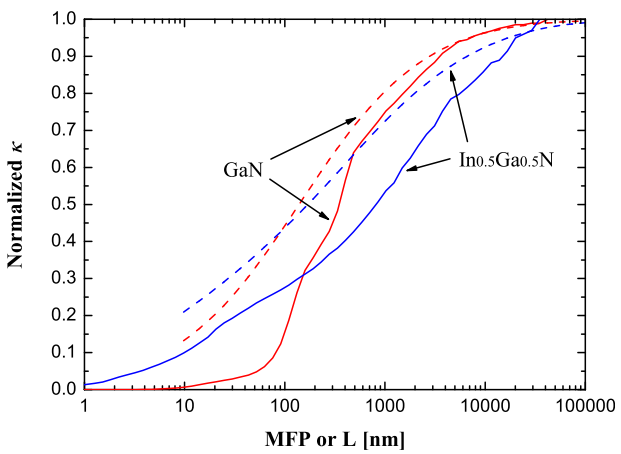

FIG. 4. Solid lines: normalized cumulative a-axis thermal conductivities of bulk GaN and $In_{0.5}Ga_{0.5}N$ as a function of mean free path at room temperature. Dashed lines: normalized room-temperature a-axis thermal conductivities of GaN and $In_{0.5}Ga_{0.5}N$ with respect to film thickness.

IV. CONCLUSION

We have predicted evident anisotropy in thermal conductivities at room temperature of wurtzite GaN, with 244 and 279 $W\,m^{-1}\,K^{-1}$ along the a-axis and c-axis, respectively, and the anisotropy is caused mainly by the high-transverse acoustic phonons. We have also studied the thermal conductivities of $Al_xGa_{1-x}N$, $In_xGa_{1-x}N$, and $In_xAl_{1-x}N$ alloys. It is found that a small amount of alloying can reduce the thermal conductivities of AlN, GaN, and InN significantly, but the thermal conductivities remain almost unaffected when the alloying concentration varies between 0.2 and 0.8. The size effect can persist up to a few tens of micrometers, and thermal conductivity can be reduced by half in about 100 nm thick films. Due to increased relative contribution from large mean-free-path phonons in alloys, the size effect is stronger in alloys than in pure compounds in thick samples; however, it is weaker in alloys than in pure compounds in thin samples.

ACKNOWLEDGMENTS

The authors thank Dr. Natalio Mingo for assistance of the relevant IFCs calculation. J. Ma and X. Luo acknowledge supports from National Nature Science Foundation of China (Nos. 51576078 and 51376070).

[1]W. Chikhaoui, J.-M. Bluet, M.-A. Poisson, N. Sarazin, C. Dua, and C. Bru-Chevallier, Appl. Phys. Lett. **96**, 072107 (2010).
[2]S. Ganguly, A. Konar, Z. Hu, H. Xing, and D. Jena, Appl. Phys. Lett. **101**, 253519 (2012).
[3]A. Sasikumar, A. R. Arehart, S. Martin-Horcajo, M. F. Romero, Y. Pei, D. Brown, F. Recht, M. A. di Forte-Poisson, F. Calle, M. J. Tadjer, S. Keller, S. P. DenBaars, U. K. Mishra, and S. A. Ringel, Appl. Phys. Lett. **103**, 033509 (2013).
[4]S.-N. Lee, H. S. Paek, H. Kim, T. Jang, and Y. Park, Appl. Phys. Lett. **92**, 081107 (2008).
[5]X. H. Wang, L. W. Guo, H. Q. Jia, Z. G. Xing, Y. Wang, X. J. Pei, J. M. Zhou, and H. Chen, Appl. Phys. Lett. **94**, 111913 (2009).
[6]C. B. Soh, W. Liu, S. J. Chua, S. S. Ang, R. J. N. Tan, and S. Y. Chow, J. Appl. Phys. **108**, 093501 (2010).
[7]S. Nakamura, M. Senoh, S. Nagahama, N. Iwasa, T. Yamada, T. Matsushita, Y. Sugimoto, and H. Kiyoku, Appl. Phys. Lett. **69**, 4056 (1996).
[8]T. Akasaka, T. Nishida, T. Makimoto, and N. Kobayashi, Appl. Phys. Lett. **84**, 4104 (2004).
[9]S.-H. Yen and Y.-K. Kuo, J. Appl. Phys. **103**, 103115 (2008).
[10]X. Zheng, R.-H. Horng, D.-S. Wuu, M.-T. Chu, W.-Y. Liao, M.-H. Wu, R.-M. Lin, and Y.-C. Lu, Appl. Phys. Lett. **93**, 261108 (2008).
[11]E. Matioli, C. Neufeld, M. Iza, S. C. Cruz, A. A. Al-Heji, X. Chen, R. M. Farrell, S. Keller, S. DenBaars, U. Mishra, S. Nakamura, J. Speck, and C. Weisbuch, Appl. Phys. Lett. **98**, 021102 (2011).
[12]S.-B. Choi, J.-P. Shim, D.-M. Kim, H.-I. Jeong, Y.-D. Jho, Y.-H. Song, and D.-S. Lee, Appl. Phys. Lett. **103**, 033901 (2013).
[13]B. C. Daly, H. J. Maris, A. V. Nurmikko, M. Kuball, and J. Han, J. Appl. Phys. **92**, 3820 (2002).
[14]W. Liu and A. A. Balandin, Appl. Phys. Lett. **85**, 5230 (2004).
[15]W. Liu and A. A. Balandin, J. Appl. Phys. **97**, 073710 (2005).
[16]B. N. Pantha, R. Dahal, J. Li, J. Y. Lin, H. X. Jiang, and G. Pomrenke, Appl. Phys. Lett. **92**, 042112 (2008).
[17]A. Sztein, H. Ohta, J. E. Bowers, S. P. DenBaars, and S. Nakamura, J. Appl. Phys. **110**, 123709 (2011).
[18]T. Tong, D. Fu, A. X. Levander, W. J. Schaff, B. N. Pantha, N. Lu, B. Liu, I. Ferguson, R. Zhang, J. Y. Lin, H. X. Jiang, J. Wu, and D. G. Cahill, Appl. Phys. Lett. **102**, 121906 (2013).

[19]H. Tong, J. Zhang, G. Liu, J. A. Herbsommer, G. S. Huang, and N. Tansu, Appl. Phys. Lett. **97**, 112105 (2010).
[20]A. Sztein, J. E. Bowers, S. P. DenBaars, and S. Nakamura, J. Appl. Phys. **112**, 083716 (2012).
[21]D. A. Broido, M. Malorny, G. Birner, N. Mingo, and D. A. Stewart, Appl. Phys. Lett. **91**, 231922 (2007).
[22]A. Ward, D. Broido, D. Stewart, and G. Deinzer, Phys. Rev. B **80**, 125203 (2009).
[23]W. Li and N. Mingo, J. Appl. Phys. **114**, 183505 (2013).
[24]L. Lindsay, D. Broido, and T. Reinecke, Phys. Rev. B **87**, 165201 (2013).
[25]J. Ma, W. Li, and X. Luo, Appl. Phys. Lett. **105**, 082103 (2014).
[26]A. X. Levander, T. Tong, K. M. Yu, J. Suh, D. Fu, R. Zhang, H. Lu, W. J. Schaff, O. Dubon, W. Walukiewicz, D. G. Cahill, and J. Wu, Appl. Phys. Lett. **98**, 012108 (2011).
[27]J. Garg, N. Bonini, B. Kozinsky, and N. Marzari, Phys. Rev. Lett. **106**, 045901 (2011).
[28]Z. Tian, J. Garg, K. Esfarjani, T. Shiga, J. Shiomi, and G. Chen, Phys. Rev. B **85**, 184303 (2012).
[29]W. Li, L. Lindsay, D. Broido, D. Stewart, and N. Mingo, Phys. Rev. B **86**, 174307 (2012).
[30]W. Li, J. Carrete, N. A. Katcho, and N. Mingo, Comput. Phys. Commun. **185**, 1747 (2014).
[31]W. Li, N. Mingo, L. Lindsay, D. Broido, D. Stewart, and N. Katcho, Phys. Rev. B **85**, 195436 (2012).
[32]J. M. Ziman, *Electrons and Phonons: The Theory of Transport Phenomena in Solids* (Oxford University Press, 2001).
[33]Z. Wang and N. Mingo, Appl. Phys. Lett. **99**, 101903 (2011).
[34]P. E. Blöchl, Phys. Rev. B **50**, 17953 (1994).
[35]J. P. Perdew and A. Zunger, Phys. Rev. B **23**, 5048 (1981).
[36]G. Kresse and J. Furthmüller, Phys. Rev. B **54**, 11169 (1996).
[37]A. Togo, F. Oba, and I. Tanaka, Phys. Rev. B **78**, 134106 (2008).
[38]M. Schwoerer-Bohning, A. T. Macrander, M. Pabst, and P. Pavone, Phys. Status Solidi B **215**, 177 (1999).
[39]H. Schulz and K. Thiemann, Solid State Commun. **23**, 815 (1977).
[40]T. Ruf, J. Serrano, M. Cardona, P. Pavone, M. Pabst, M. Krisch, M. D'Astuto, T. Suski, I. Grzegory, and M. Leszczynski, Phys. Rev. Lett. **86**, 906 (2001).
[41]J. M. Zhang, T. Ruf, M. Cardona, O. Ambacher, M. Stutzmann, J.-M. Wagner, and F. Bechstedt, Phys. Rev. B **56**, 14399 (1997).
[42]A. Jeówski, B. Danilchenko, M. Boḱowski, I. Grzegory, S. Krukowski, T. Suski, and T. Paszkiewicz, Solid State Commun. **128**, 69 (2003).
[43]L. Lindsay, D. Broido, and T. Reinecke, Phys. Rev. Lett. **109**, 095901 (2012).
[44]W. Li and N. Mingo, J. Appl. Phys. **114**, 054307 (2013).
[45]J. Chen, G. Zhang, and B. Li, Appl. Phys. Lett. **95**, 073117 (2009).